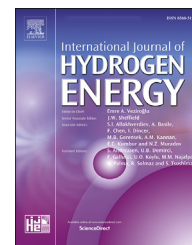




ELSEVIER

Available online at www.sciencedirect.com

ScienceDirect

journal homepage: www.elsevier.com/locate/he

Plasmonic nickel nanoparticles decorated on to LaFeO₃ photocathode for enhanced solar hydrogen generation

Govinder Singh Pawar^a, Ameen Elikkottil^{b,c}, Bala Pesala^{b,c},
Asif Ali Tahir^{a,*}, Tapas Kumar Mallick^a

^a Environment and Sustainability Institute, University of Exeter, Penryn, Cornwall, TR10 9FE, United Kingdom

^b Academy of Scientific and Innovative Research (AcSIR), Taramani, Chennai, 600113, India

^c CSIR – Structural Engineering Research Centre (CSIR-SERC), Taramani, Chennai, 600113, India

ARTICLE INFO

Article history:

Received 5 September 2018

Received in revised form

29 October 2018

Accepted 31 October 2018

Available online xxx

Keywords:

Photoelectrochemical water splitting

Surface plasmon resonance

Ni nanoparticle

Finite difference time domain

Photocathode

LaFeO₃

ABSTRACT

Plasmonic Ni nanoparticles were incorporated into LaFeO₃ photocathode (LFO-Ni) to excite the surface plasmon resonances (SPR) for enhanced light harvesting for enhancing the photoelectrochemical (PEC) hydrogen evolution reaction. The nanostructured LFO photocathode was prepared by spray pyrolysis method and Ni nanoparticles were incorporated on to the photocathode by spin coating technique. The LFO-Ni photocathode demonstrated strong optical absorption and higher current density where the untreated LFO film exhibited a maximum photocurrent of 0.036 mA/cm² at 0.6 V vs RHE, and when incorporating 2.84 mmol Ni nanoparticles the photocurrent density reached a maximum of 0.066 mA/cm² at 0.6 V vs RHE due to the SPR effect. This subsequently led to enhanced hydrogen production, where more than double (2.64 times) the amount of hydrogen was generated compared to the untreated LFO photocathode. Ni nanoparticles were modelled using Finite Difference Time Domain (FDTD) analysis and the results showed optimal particle size in the range of 70–100 nm for Surface Plasmon Resonance (SPR) enhancement.

© 2018 Hydrogen Energy Publications LLC. Published by Elsevier Ltd. All rights reserved.

Introduction

With climate change and global warming ever becoming the focus of concern for millions of people globally, there is a critical need to develop scalable and sustainable energy source assets. One of the possible way this can be accomplished is by harnessing the solar energy reaching the earth's surface, which supplies enough energy every hour to meet humanities need for a year [1]. However, the predominant

renewable energy sources, solar energy and wind energy, are highly intermittent and hence there is a dire need for the development of sustainable energy storage systems. The conversion of incoming photons from the sun light into storable chemical fuel (hydrogen), also known as solar fuel, is a highly attractive clean and sustainable energy storage solution. The stored hydrogen can be converted to electricity as per the demand using fuel cells.

Currently, the major processes being explored for hydrogen generation are steam reforming [2,3], coal

* Corresponding author.

E-mail addresses: A.Tahir@exeter.ac.uk, asifali_tahir@hotmail.com (A.A. Tahir).

<https://doi.org/10.1016/j.ijhydene.2018.10.240>

0360-3199/© 2018 Hydrogen Energy Publications LLC. Published by Elsevier Ltd. All rights reserved.

gasification [4], biomass derivatives [5], thermochemical [6] and biological processes [7]. However, most of these processes are energy intensive and generates a large carbon footprint. Photoelectrochemical (PEC) water splitting is a potential pathway in realising environmental friendly hydrogen production as it only requires semiconductor electrodes, water and sunlight [8]. The semiconductor materials require favourable band alignments for water reduction/oxidation, optimal bandgaps and high stability under reaction conditions [9]. Cu_2O [10,11], WSe_2 [12], CdTe [13], CuGaSe_2 [8], Si [14], GaP [15] and InP [16] are photocathode materials which already have applications in solar assisted water splitting for hydrogen generation. However, due to availability, cost, stability and synthesis procedures there are limitations to their use. LaFeO_3 (LFO), a non-toxic p-type semiconductor material with a direct bandgap of 2.4 eV, high stability and ability to generate hydrogen spontaneously without the need of an external bias [17], is a promising photocathode material for solar to hydrogen conversion. However, due to its low absorption coefficient, the current density is low, thus yielding lower amounts of hydrogen. Therefore, improving the material's light extracting ability is crucial for improving the hydrogen yield capability of LFO.

Metallic nanoparticles based on gold (Au) and silver (Ag), have the ability for enhancing optical extinction (scattering and absorption) by excitation of Surface Plasmon Resonance (SPR). In metallic nanoparticles, light driven oscillations of conduction electrons cause oscillating dipoles which in turn excite strong SPR at the right wavelengths [18]. Optimized nanoparticles results in higher surface electro-magnetic fields leading to higher extinction cross-section, much larger than geometric cross-section [19]. The enhanced electromagnetic field is dependent upon the wavelength of incident light, shape, size and aggregation state of the nanoparticles [20]. There are three methods of plasmonic light-trapping geometries: 1) Far-Field scattering, 2) Near-Field scattering and 3) Surface plasmon polaritons at the metal/semiconductor interface [21]. Zhang et al. [22] showed that upon incorporating Au nanocrystals on to TiO_2 nanotubes, the photocurrent density almost doubles compared to the untreated TiO_2 nanotubes, due to SPR effect. This subsequently led to high hydrogen yield, 27.9 $\mu\text{mol/h}$. Lian et al. [23] showed improved current density of three times with vast improvement of hydrogen yield compared to untreated TiO_2 nanotubes, more than 20 times, again due to SPR effect. Pawar et al. [24] showed improved current densities of more than two times when Ag nanoparticles were incorporated onto LFO films leading to over twice the amount of hydrogen generated compared to its untreated counterpart. Therefore, SPR is a potential method of improving a semiconductors light harvesting ability to improve its hydrogen production yield. However, both Au and Ag are costly and would drive up the cost of fabricating a photoelectrode, especially on an industrial scale.

Nickel (Ni), one of the earth's most abundant elements, has been receiving a lot of attention due to its lower cost, electrochemical stability and availability. It has shown the ability to enhance hydrogen evolution when deposited on to graphene sheets [25,26], crystalline silicon electrodes [27] and metal oxides [9]. Nickel nanoparticles have managed to improve the current density and hydrogen yield of these

materials. Compared to strong SPR effect in Au and Ag nanoparticles, relatively weak SPR effect in Ni nanoparticles is less explored [28,29]. Amekura et al. [30] conducted an experiment where they embedded Ni nanoparticles into silica glass and identified the absorption peaks due to SPR effect from the Ni nanoparticles. This shows that Ni nanoparticles have the potential to improve a semiconductor's light harvesting ability by SPR, thus improving the current density and hydrogen generation performance. Therefore, Ni nanoparticle based LFO photocathode is prepared and performance evaluation is carried out to determine the enhancement in its photocurrent and hydrogen yield.

Herein, we report the design and fabrication of LFO-Ni photocathode and its performance. Finite Difference Time Domain (FDTD) simulations are employed to simulate the SPR resonances of Ni nanoparticles. The FDTD simulations show that the Ni nanoparticles with diameters in the range of 70–100 nm demonstrate good SPR effect suitable for incorporation with LFO photocathodes. Experimentally, these nanoparticles show enhanced light harvesting capabilities leading to higher photocurrent densities and greater hydrogen yield. To the best of our knowledge, this is the first time LFO-Ni photocathode has been synthesised leading to increased hydrogen production, due to SPR, when compared to its untreated counterpart.

Method

FDTD simulations

The spectral response of Ni nanoparticle is studied using Finite Difference Time Domain (FDTD) simulation tool from Lumerical. Palik refractive index database is used for Ni in the simulations. The simulation background is set as water with refractive index to mimic dilute NaOH (0.1 M NaOH in water). A total field scattering field source is used for simulations with a wavelength range of 300–700 nm. The simulations employs a perfectly matched layer boundary conditions with symmetric in x direction and anti-symmetric in z direction. Mesh size is set to 0.5 nm and the diameter of the nanoparticle is varied from 70 nm to 150 nm in steps of 10 nm to simulate the surface plasmon resonances and to quantify the enhancement in optical extinction coefficients.

Preparation of LFO-Ni photocathode

The LaFeO_3 photocathode was fabricated using spray pyrolysis method, where full details of the experimental procedure can be found in our previous work [17]. The Nickel nanoparticles (from Sigma Aldrich, where average particle size is ≤ 100 nm) were incorporated into the LFO films by spin coating method. The Ni nanopowder (2.84 mmol) is placed into a vial containing acetone. Subsequently, it was ultrasonicated for 2 h to break down any large particles and for obtaining a homogeneous suspension of Ni nanoparticles in acetone. The concentrated Ni nanoparticle suspension was serially diluted to obtain a concentration of 1.42 mmol for electrode performance evaluation. In addition to this, a higher concentration of 5.68 mmol solution was also prepared. A

strip of Kapton tape was pasted on to FTO glass for electrical contact. Three different electrodes were prepared with these Ni nanoparticle solutions of various concentrations by spin coating at 500 rpm for 30 s. These electrodes were then annealed at a low temperature of 50 °C for 15 min. This ensures the evaporation of acetone and enhances the binding of Ni nanoparticles to the film without their oxidation.

Instrument details

Material characterization

The material phase composition was determined using a Bruker D8 Advance X-Ray Diffractometer (XRD) (Cu K α irradiation, 40 kV/40 mA, 0.02° 2 θ step and a scan time of 3 s per step) in the range of 20–70° 2 θ . The morphology and composition of the thin film was characterized using a high resolution Scanning Electron Microscope (SEM, HITACHI S3200N) coupled with an Energy Dispersive Spectroscopy (EDS, Oxford instrument elemental analysis). Diffuse reflectance spectra was acquired using a spectrophotometer (PerkinElmer lambda 1050 with 150 mm integrated InGaAs sphere and PbS detector).

Electrochemical characterization

All electrochemical experiments were carried out in a standard 3 electrode system, composed of a working electrode, Pt wire as counter electrode and a reference electrode of Ag/AgCl in saturated KCl. The data collection was carried out using potentiostat (Metrohm Autolab PGSTAT302N). The working electrode potential versus the Ag/AgCl reference electrode used in all experiments was converted into the Reversible Hydrogen Electrode (RHE) using equation: $V_{\text{RHE}} = V_{\text{Ag/AgCl}} + 0.197 \text{ V} + 0.059 \text{ V} \cdot \text{pH}$.

The photoelectrochemical (PEC) performance of LaFeO₃ and LaFeO₃-Ni photoelectrodes were measured in 0.1 M NaOH aqueous solution (pH 13) under light illumination using a 300 W ozone free Xenon lamp equipped with an AM 1.5 filter (Newport 66902). A one sun illumination (100 mW/cm²) is used. A Linear Sweep Voltammetry (LSV) scan in the positive to negative direction between the ranges of +0.35 V to -0.7 V is done.

Chronoamperometric (CA) measurements of LaFeO₃ and LaFeO₃-Ni photocathodes were conducted over a period of 20 h under a continuous 1 sun illumination. This was carried out in 0.1 M NaOH (pH 13) aqueous solution with no sacrificial agents, in a standard 3 electrode system in ambient atmosphere and temperature. A constant voltage of 0 V was maintained over the measurement period.

Hydrogen evolution measurements

Gas Chromatography (GC) measurements were carried out using a manual injection GC system (PerkinElmer Clarus 580) using a molecular sieve (PerkinElmer) and a Pulsed Discharge Detector (PDD) with an argon flow of 28 ml min⁻¹. A custom-made glass reactor vessel with an attached fused silica viewport containing 0.1 M NaOH (pH 13) with a dead

space of 100 ml was purged with argon for 2 h with gentle heating and stirring to remove atmospheric air from the system. The sealed vessel contained the working LaFeO₃ electrode connected to a Pt mesh by a single outer wire and was subjected to light illumination for the water splitting reaction. GC measurements were carried at an interval of 1 h.

Results and discussion

FDTD simulations: extinction, absorption and scattering

Extinction, absorption and scattering cross-sections of Ni nanoparticle of varying diameter is shown in Fig. 1 (a) to 1 (i). The results show broad peaks in extinction and scattering, which red shift with the increase in size of the nanoparticle. For particle diameters greater than 110 nm, the scattering cross-section dominate over the absorption cross-section. The extinction cross-section is more than 3.5 times than the geometrical cross-section for Ni nanoparticle of diameter greater than 90 nm. It should be noted that the polarizability of Ni is weak compared to conventional noble metals such as Au and Ag, hence this results in weaker surface plasmon resonances [31,32]. Polarizability depends on the number of free electrons, nickel has less electrons compared to gold [33].

In general, the extinction cross-section increases with increase in particle diameter (Fig. 1(g)). However, the normalized absorption cross-section (Fig. 1(h)) decreases with increasing size of the nanoparticle while the normalized scattering cross-section increases (Fig. 1(i)) with increasing size of the nanoparticle. However, larger particle sizes (>100 nm) tend to agglomerate which results in decreased SPR performance [34] and hence it is recommendable to use lower size nanoparticles.

Electric field profile for Ni nanoparticle: on and OFF resonance

Ni nanoparticles exhibit localized Surface Plasmon Resonances (LSPR) in the visible frequency range. The electronic configuration of Ni is [Ar] 3d⁸ 4s². The plasmonic resonance happens due to the oscillations of the electron cloud caused by the incident electromagnetic radiation. The electron oscillations are maximum at the SPR resonance frequency (ON resonance) and are weak away from the SPR (OFF resonance).

Maximum extinction occurs at a wavelength region of 390–540 nm for a Ni nanoparticle with size varying in the range of 70–120 nm (Fig. 1(i)). To understand electric field enhancements at SPR, simulations are carried out for a 100 nm size Ni nanoparticle. Fig. 2(a) shows the high electric field at the ON resonance wavelength of 462.7 nm. The electric field profile at OFF resonance wavelength of 300 nm show low enhancement in electric field (Fig. 2(b)). The electric field enhancement at ON resonance (Fig. 2(a)) is ~3 times compared to the OFF resonance. The SPR enhancement will enable the photocathode to harness more light through increased optical absorption and scattering and is expected to result in higher hydrogen evolution.

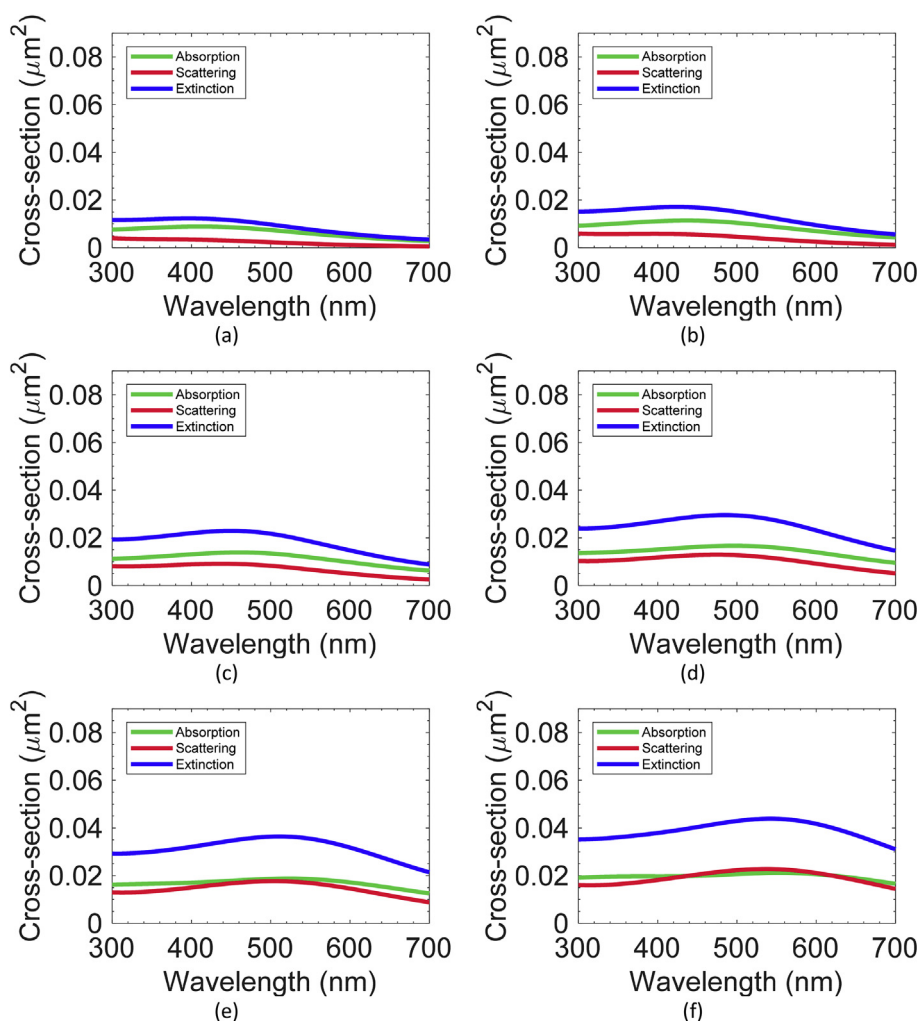


Fig. 1 – Extinction, Absorption and Scattering cross sections of Ni nanoparticles of diameters (a) 70 nm (b) 80 nm (c) 90 nm (d) 100 nm (e) 110 nm (f) 120 nm (g) normalized extinction cross-section (h) normalized absorption cross-section (i) normalized scattering cross-section.

Performance and characterization of LFO-Ni photocathode

LFO films were prepared by spray pyrolysis of the precursor solution at 150 °C and then post-annealing at 550 °C in air, to obtain a single-phase crystalline material. The optimized size of Ni nanoparticle from theoretical modelling is close to 100 nm (as larger nanoparticles will tend to agglomerate) and hence similar nanoparticle range is used in the fabrication of LFO-Ni. Ni nanoparticles at varying concentrations (LFO-Ni 5.68 mmol, LFO-Ni 2.84 mmol and LFO-Ni 1.42 mmol) were prepared by spin coating the Ni nanoparticle solutions on to the pre-prepared LFO films to determine the optimum concentration of Ni nanoparticles required to give the best performance. The PEC performance of the LFO-Ni films were performed in 0.1 M aqueous NaOH (pH 13) solution by illuminating the photocathode from the electrolyte side to evaluate the current density, compared to plain LFO photocathode. The photocurrent density (j) is plotted against bias potential (V) as shown in Fig. 3. The untreated LFO film exhibited a maximum photocurrent of 0.036 mA/cm² at 0.6 V vs RHE. Upon incorporating 2.84 mmol Ni nanoparticles, there

is a distinct improvement of the photocurrent density where it reaches a maximum of 0.066 mA/cm² at 0.6 V vs RHE due to the SPR effect. When increasing the concentration of Ni nanoparticles, a decrease in current density is observed between the range of 0.7–1 V vs RHE by 10%. This decrease can be due to the higher content of Ni nanoparticles on the film surface reducing the electrode/electrolyte interface inhibiting effective charge separation, thus decreasing the amount of current density. As the Ni nanoparticle concentration is reduced to 1.42 mmol, there is also a decrease in photocurrent between the ranges of 0.7–1 V vs RHE by 7%. This can be due to lower amount Ni nanoparticle on the film available for SPR enhancement. Although the maximum current density for 1.42 mmol is higher than for the 2.84 mmol film, it is lower overall through the range. Therefore, from the entire three measured concentrations 2.84 mmol Ni nanoparticle could result in the maximum overall yield.

Chronoamperometric (CA) measurements of both LFO and best performing LFO-Ni (2.84 mmol) photocathodes were conducted in a 0.1 M NaOH aqueous electrolyte solution over a period of 20 h with continuous illumination. A constant

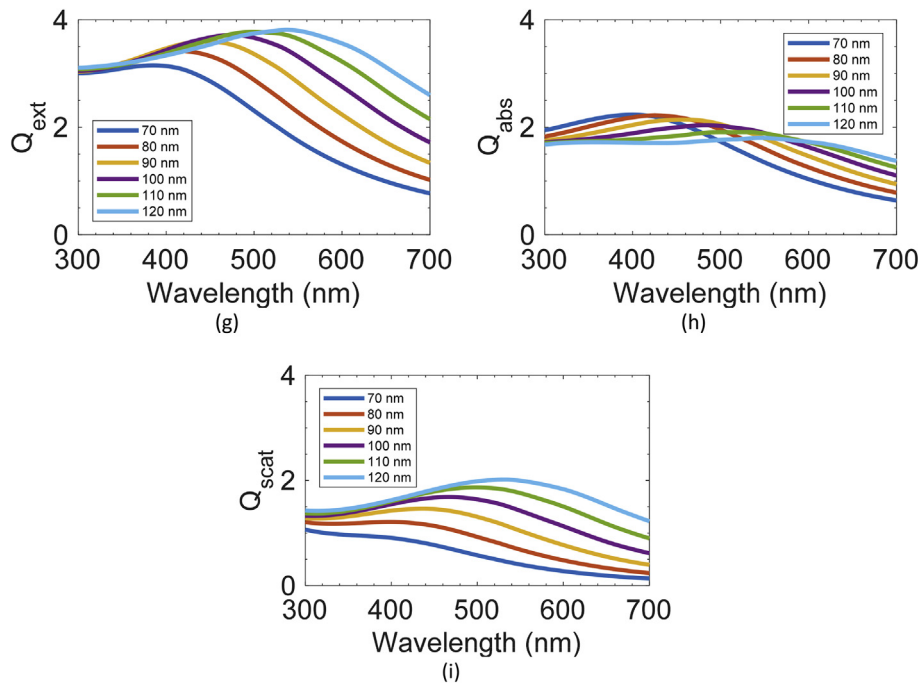


Fig. 1 – (continued).

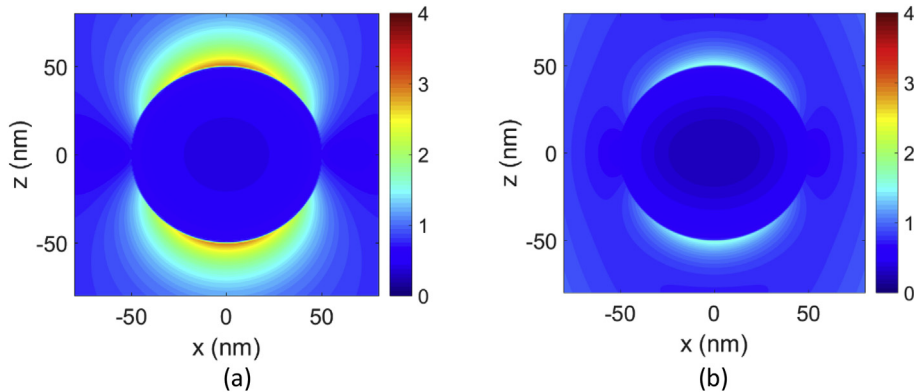


Fig. 2 – Electric Field Intensity of 100 nm Ni nanoparticle at wavelengths (a) 462.7 nm (ON Resonance) (b) 300 nm (OFF Resonance).

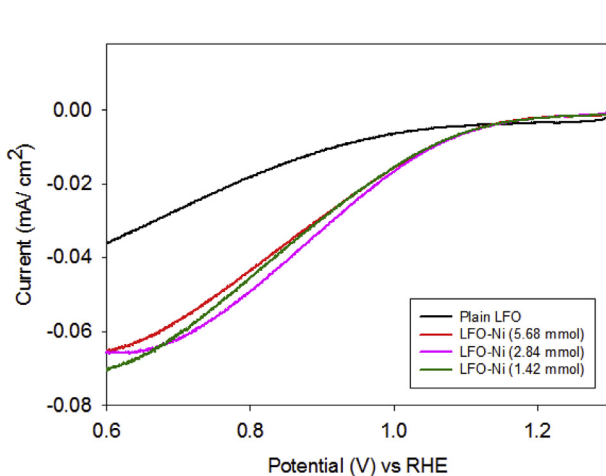


Fig. 3 – J-V characteristics of plain LFO and various LFO-Ni concentrations in a 0.1 M NaOH electrolyte vs RHE.

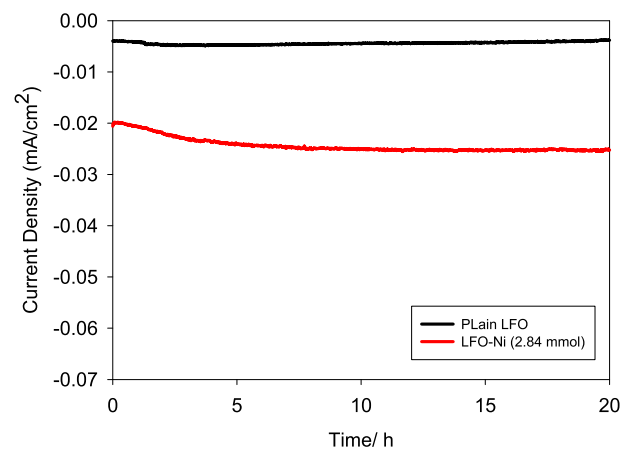


Fig. 4 – Chronoamperometric measurement of LFO and LFO-Ni (2.84 mmol) photocathodes in an aqueous 0.1 M NaOH electrolyte solution at 0 V vs Ag/AgCl.

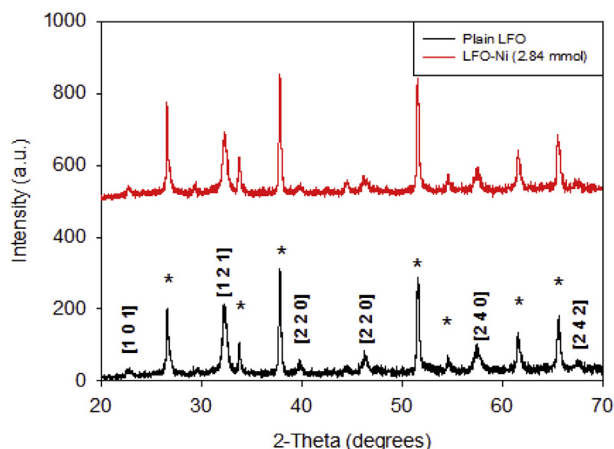


Fig. 5 – XRD pattern of plain LFO (black solid line) and LFO-Ni (2.84 mmol), red solid line, on FTO glass substrate. The peaks marked with asterisk represent FTO. (For interpretation of the references to color in this figure legend, the reader is referred to the Web version of this article.)

potential of 0 V was maintained during the course of the experiment. Fig. 4 shows the stability performances of both photocathodes. As observed, both the photocathodes are very stable for the duration of the experiment, showing very little signs of current degradation. Most importantly, the current density of LFO-Ni (2.84 mmol) is over six times than that of plain LFO. This shows that with the incorporation of Ni nanoparticles on to the film, it greatly improves the current generated without losing stability. Therefore, we would expect an increase in hydrogen yield compared to that of plain LFO.

LFO-Ni (2.84 mmol), the best performing photocathode, is taken to identify its crystal phase compared to its untreated counterpart. The XRD pattern for both photocathodes are shown in Fig. 5. The XRD patterns exhibits crystalline single phase peaks for plain LFO film with the LFO particles orientated in the (121) plane, which is in good agreement with previous works [17]. All the peaks correspond to LFO are indexed to orthorhombic system (JCPDS 00-037-1439). No Ni diffraction peaks were detected in the LFO-Ni film, which can be due to small particle size, dispersity or low Ni nanoparticle loading content. We would expect there to be three characteristic Ni peaks at 44.5, 51.8 and 76.4 considering bulk material [35,36]. Peaks marked with an asterisk correspond to the FTO peaks, distinguishing it from the LFO peaks.

Fig. 6 shows the top view SEM of the plain LFO and LFO-Ni (2.84 mmol) films. The plain LFO nanostructured film (Fig. 6(a)) shows well connected crystal grain structure, post annealing at 550 °C. Its EDS (Fig. 6(c)) confirms that there is no Ni nanoparticle present on the film. Fig. 6(b) shows bright spherical nanoparticles distributed across the film which can be attributed to the Ni nanoparticles confirmed by its EDS (Fig. 6(d)). Comparing images 6(a) and (b), it can be seen that Ni nanoparticle have been incorporated into the LFO film after spin coating, which is further confirmed by their respective EDS analysis.

To understand the effect of Ni nanoparticles on light absorption, its optical properties were measured using UV-Vis spectroscopy. Fig. 7 shows the absorption spectra of both plain LFO and LFO-Ni (2.84 mmol) at wavelengths from 360 to 800 nm. There was a higher absorption of light in the short wavelength (400–600 nm) and a slight increase in the long wavelength region (600–800 nm), which can be attributed to increased light extinction from the Ni nanoparticle in this

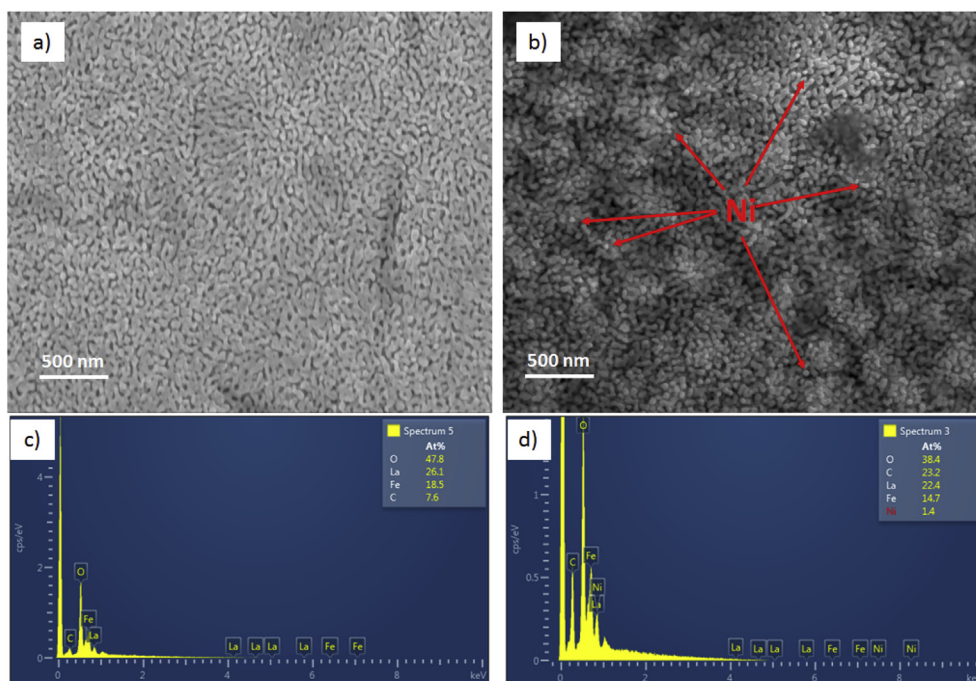


Fig. 6 – (a) Top view SEM of plain LFO film, (b) top view SEM of LFO-Ni (2.84 mmol), (c) EDS for plain LFO film and (d) EDS for LFO-Ni (2.84 mmol).

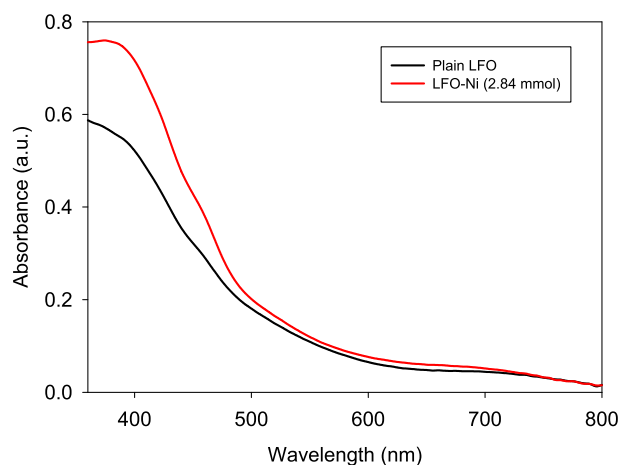


Fig. 7 – Absorbance spectra of plain LFO and LFO-Ni (2.84 mmol).

frequency range due to SPR effect. The SPR effect results in higher effective absorption of light in the semiconductor due to light concentration which increases the electron-hole generation in the semiconductor [37], PIRET (Plasmon induced Resonance Energy Transfer) through dipole-dipole interaction and light scattering which results in increased effective optical path length. In addition, NPs at the semiconductor-electrolyte can also increase the catalytic effects. The relative contribution of each of these effects in our Ni incorporated LFO films requires further detailed study.

By incorporating Ni nanoparticles on to the LFO film, we observe an enhancement of light harvesting capability compared to plain LFO. This is seconded by the increase in current density in case of PEC performance (Fig. 3). Therefore, a higher volume of hydrogen is expected to be obtained from the solar water splitting experiment. As the photocathode absorbs more light, it generates more current for water splitting, thus yielding a greater volume of hydrogen.

Hydrogen evolution measurements were conducted in an aqueous 0.1 M NaOH solution under constant illumination, for the plain LFO film and for various LFO-Ni films (Fig. 8). The

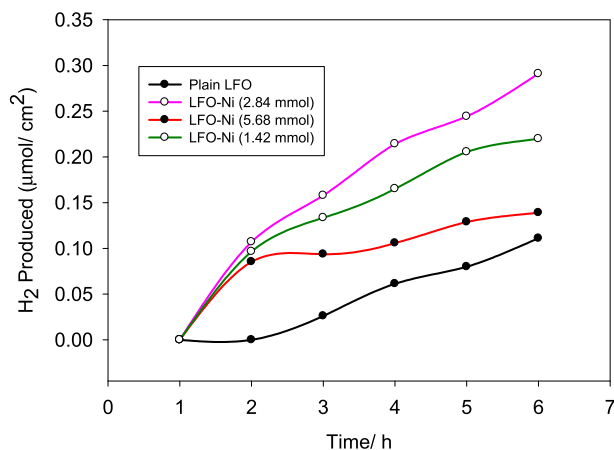


Fig. 8 – Hydrogen evolution test of plain LFO and LFO-Ni with varying Ni concentrations, in an aqueous 0.1 M NaOH solution.

water splitting test was conducted in a custom made glass reactor vessel with an attached fused silica viewport, described in our previous work [17]. The working electrode and Pt counter electrode were connected by a single looped wire, without any external bias being applied. After 3 h, the plain LFO photocathode begins spontaneously producing hydrogen via solar water splitting. After 6 h of reaction time, it has generated $0.11 \mu\text{mol}/\text{cm}^2$ of hydrogen. On the other hand, all of the LFO-Ni photocathodes begun spontaneously generating hydrogen after 2 h of reaction time. This is a marked improvement compared to the untreated LFO. This improvement can be ascribed due to the SPR effect of Ni nanoparticles resulting in enhanced light harvesting capability of the photoelectrode, where it produces more electrons available for conversion to hydrogen. This is in good agreement with the *J-V* curves seen in Fig. 3. As 2.84 mmol of Ni nanoparticle is incorporated into the film, there is an increase in current, which subsequently leads to an increase in hydrogen yield; after 6 h $0.29 \mu\text{mol}/\text{cm}^2$ is produced. This is an improvement of more than two times. As the Ni concentration is reduced to 1.42 mmol, there is a decrease in current leading to a drop in hydrogen yield where at 6 h it generates $0.22 \mu\text{mol}/\text{cm}^2$. Due to lower Ni content there is less light being trapped due to plasmonic effect so less electrons are generated thus leading to the drop in hydrogen yield compare to LFO-Ni (2.84 mmol) respectively. When the concentration of Ni is increased to 5.68 mmol as expected there is a decrease in hydrogen yield, after 6 h it has only generated $0.14 \mu\text{mol}/\text{cm}^2$. This will be due to the higher content of Ni nanoparticles on the film surface reducing the electrode/electrolyte interface inhibiting effective charge separation, or the Ni nanoparticles agglomerating lowering its effective surface area. Therefore, the optimal concentration of Ni nanoparticle for improved current and hydrogen yield is 2.84 mmol.

Conclusion

In summary, we have incorporated optimized Ni nanoparticles (of diameters ranging from 70 to 100 nm) on to the nanostructured LFO photocathode. The photocathode shows an increase of light absorption upon incorporating Ni nanoparticles compared to its untreated counterpart. This agrees well with FDTD studies, which shows good light harvesting ability of Ni nanoparticles of small sizes ranging from 70 to 100 nm, where there will be lower chances of aggregation. Incorporation of Ni nanoparticle has increased the current density, where the best performing LFO-Ni (2.84 mmol) photocathode generated more than twice the current density compared to plain LFO, due to the SPR effect from Ni nanoparticles. This subsequently led to the LFO-Ni (2.84 mmol) photocathode producing more than double (2.64 times) the amount of hydrogen compared to the plain LFO. The optimized photocathode generated $0.29 \mu\text{mol}/\text{cm}^2$ hydrogen after 6 h of operation whereas the plain LFO only generated $0.11 \mu\text{mol}/\text{cm}^2$. Furthermore, the LFO-Ni photocathodes were able to produce hydrogen after 2 h of illumination compared to the untreated LFO photocathode, which began forming hydrogen only after 3 h of illumination. This finding shows that Ni nanoparticles are able to enhance the

performance of LFO photocathodes plasmonically in a much more cost effective manner compared to Ag and Au.

Acknowledgement

We acknowledge UKIERI-DST 2016-17-0089 project and Engineering and Physical Science Research Council, UK (EPSRC) under the research grant EP/R512801/1 for financial support. A.E. would like to thank the Council of Scientific and Industrial Research (CSIR) for the award of Senior Research Fellowship. NSG Pilkington Glass Ltd. is acknowledged for kindly providing the FTO substrates for this work.

Appendix A. Supplementary data

Supplementary data to this article can be found online at <https://doi.org/10.1016/j.ijhydene.2018.10.240>.

REFERENCES

- [1] Schiermeier Q, Tollefson J, Scully T, Witze A, Morton O. Energy alternatives: electricity without carbon. *Nature* 2008;454(7206):816–23.
- [2] Zhang B, Tang X, Li Y, Xu Y, Shen W. Hydrogen production from steam reforming of ethanol and glycerol over ceria-supported metal catalysts. *Int J Hydrogen Energy* 2007;32(13):2367–73.
- [3] Ochoa-Fernández E, Rusten HK, Jakobsen HA, Rønning M, Holmen A, Chen D. Sorption enhanced hydrogen production by steam methane reforming using Li₂ZrO₃ as sorbent: sorption kinetics and reactor simulation. *Catal Today* 2005;106(1–4):41–6.
- [4] Nowotny J, Sorrell CC, Sheppard LR, Bak T. Solar-hydrogen: environmentally safe fuel for the future. *Int J Hydrogen Energy* 2005;30(5):521–44.
- [5] Lu X, Xie S, Yang H, Tong Y, Ji H. Photoelectrochemical hydrogen production from biomass derivatives and water. *Chem Soc Rev* 2014;43(22):7581–93.
- [6] Czernik S, Evans R, French R. Hydrogen from biomass-production by steam reforming of biomass pyrolysis oil. *Catal Today* 2007;129(3–4):265–8.
- [7] Ni M, Leung DYC, Leung MKH, Sumathy K. An overview of hydrogen production from biomass. *Fuel Process Technol* 2006;87(5):461–72.
- [8] Moriya M, Minegishi T, Kumagai H, Katayama M, Kubota J, Domen K. Stable hydrogen evolution from CdS-modified CuGaSe₂ photoelectrode under visible-light irradiation. *J Am Chem Soc* 2013;135(10):3733–5.
- [9] Dubale AA, Pan C-J, Tamirat AG, Chen H-M, Su W-N, Chen C-H, et al. Heterostructured Cu₂O/CuO decorated with nickel as a highly efficient photocathode for photoelectrochemical water reduction. *J Mater Chem A* 2015;3(23):12482–99.
- [10] Luo J, Steier L, Son MK, Schreier M, Mayer MT, Grätzel M. Cu₂O nanowire photocathodes for efficient and durable solar water splitting. *Nano Lett* 2016;16(3):1848–57.
- [11] Paracchino A, Laporte V, Sivula K, Grätzel M, Thimsen E. Highly active oxide photocathode for photoelectrochemical water reduction. *Nat Mater* 2011;10(6):456–61.
- [12] McKone JR, Pieterick AP, Gray HB, Lewis NS. Hydrogen evolution from Pt/Ru-coated p-type WSe₂ photocathodes. *J Am Chem Soc* 2013;135(1):223–31.
- [13] Mathew X, Bansal A, Turner JA, Dhere R, Mathews NR, Sebastian PJ. Photoelectrochemical characterization of surface modified CdTe for hydrogen production. *J N Mater Electrochem Syst* 2002;5(2):149–54.
- [14] Lin Y, Battaglia C, Boccard M, Hettick M, Yu Z, Ballif C, et al. Amorphous Si thin film based photocathodes with high photovoltage for efficient hydrogen production. *Nano Lett* 2013;13(11):5615–8.
- [15] Liu C, Sun J, Tang J, Yang P. Zn-doped p-type gallium phosphide nanowire photocathodes from a surfactant-free solution synthesis. *Nano Lett* 2012;12(10):5407–11.
- [16] Lee MH, Takei K, Zhang J, Kapadia R, Zheng M, Chen YZ, et al. P-type InP nanopillar photocathodes for efficient solar-driven hydrogen production. *Angew Chem Int Ed* 2012;51(43):10760–4.
- [17] Pawar GS, Tahir AA. Unbiased spontaneous solar fuel production using stable LaFeO₃ photoelectrode. *Sci Rep* 2018;8(1):3501.
- [18] Si Lifang, Qiu Teng, Zhang Wenjun, Chu PK. Recent progress in design of plasmonic thin-film solar cells with enhanced efficiency. *Recent Pat Mater Sci* 2012;5(2):166–72.
- [19] Paul H, Fischer R. How can a particle absorb more than the light incident on it? *Am J Phys* 1983;51(4):323–7.
- [20] Luan X, Wang Y. Plasmon-enhanced performance of dye-sensitized solar cells based on electrodeposited Ag nanoparticles. *J Mater Sci Technol* 2014;30(1):1–7.
- [21] Atwater HA, Polman A. Plasmonics for improved photovoltaic devices. *Nat Mater* 2010;9(3):205–13.
- [22] Zhang Z, Zhang L, Hedhili MN, Zhang H, Wang P. Plasmonic gold nanocrystals coupled with photonic crystal seamlessly on TiO₂ nanotube photoelectrodes for efficient visible light photoelectrochemical water splitting. *Nano Lett* 2013;13(1):14–20.
- [23] Lian Z, Wang W, Xiao S, Li X, Cui Y, Zhang D, et al. Plasmonic silver quantum dots coupled with hierarchical TiO₂ nanotube Arrays photoelectrodes for efficient visible-light photoelectrocatalytic hydrogen evolution. *Sci Rep* 2015;5:1–10. April.
- [24] Pawar GS, Elikkottil A, Seetha S, Reddy S, Pesala B, Tahir AA, et al. Enhanced photoactivity and hydrogen generation of LaFeO₃ photocathode by plasmonic silver nanoparticle incorporation. *ACS Appl Energy Mater* 2018;1(7):3449–56.
- [25] Indra A, Menezes PW, Kailasam K, Hollmann D, Schröder M, Thomas A, et al. Nickel as a Co-catalyst for photocatalytic hydrogen evolution on graphitic-carbon nitride (Sg-CN): what is the nature of the active species? *Chem Commun* 2016;52(1):104–7.
- [26] Zhang W, Li Y, Zeng X, Peng S. Synergetic effect of metal nickel and graphene as a cocatalyst for enhanced photocatalytic hydrogen evolution via dye sensitization. *Sci Rep* 2015;5:1–12. May.
- [27] McKone JR, Warren EL, Boettcher SW, Brunschwig BS, Lewis NS, et al. Evaluation of Pt, Ni, and Ni–Mo electrocatalysts for hydrogen evolution on crystalline Si electrodes. *Energy Environ Sci* 2011;4(9):3573.
- [28] Picciotto A, Pucker G, Torrisi L, Bellutti P, Caridi F, Bagolini A. Evidence of plasmon resonances of nickel particles deposited by pulsed laser ablation. *Radiat Eff Defect Solid* 2008;163(4–6):513–8.
- [29] Dalouji V, Elahi SM, Naderi S. Surface plasmon resonance and electrical properties of RF: magnetron sputtered carbon–nickel composite films at different annealing temperatures. *Rare Met* 2016;35(11):863–9.
- [30] Amekura H, Takeda Y, Kitazawa H, Kishimoto N. Resonance energy of surface plasmon of nickel nanoparticles in silica glasses. *Photon Process Microelectron Photonics II* 2003;4977:639–47. October 2015.

- [31] Attaran A, Emami SD, Soltanian MRK, Penny R, Behbahani F, Harun SW, et al. Circuit model of fano resonance on tetramers, pentamers, and broken symmetry pentamers. *Plasmonics* 2014;9(6):1303–13.
- [32] Cuadrado A, López-Alonso JM, González FJ, Alda J. Spectral response of metallic optical antennas driven by temperature. *Plasmonics* 2017;12(3):553–61.
- [33] Chen J, Albella P, Pirzadeh Z, Alonso-González P, Huth F, Bonetti S, et al. Plasmonic nickel nanoantennas. *Small* 2011;7(16):2341–7.
- [34] Du M, Tang GH. Optical property of nanofluids with particle agglomeration. *Sol Energy* 2015;122:864–72.
- [35] Sapkal SB, Shelke KF, Shingate BB, Shingare MS. Nickel nanoparticle-catalyzed facile and efficient one-pot synthesis of polyhydroquinoline derivatives via hantzsch condensation under solvent-free conditions. *Tetrahedron Lett* 2009;50(15):1754–6.
- [36] Cheng J, Zhang X, Ye Y. Synthesis of nickel nanoparticles and carbon encapsulated nickel nanoparticles supported on carbon nanotubes. *J Solid State Chem* 2006;179(1):91–5.
- [37] Valenti M, Jonsson MP, Biskos G, Schmidt-Ott A, Smith WA. Plasmonic nanoparticle-semiconductor composites for efficient solar water splitting. *J Mater Chem A* 2016;4(46):17891–912.